NANO LETTERS

2007
Vol. 7, No. 7
2136−2141

Nanostructured Solid Oxide Fuel Cell Electrodes

T. Z. Sholklapper,*,†,‡ H. Kurokawa,† C. P. Jacobson,† S. J. Visco,† and L. C. De Jonghe†,‡

Materials Sciences Division, Lawrence Berkeley National Laboratory, Berkeley, California 94720, and Department of Materials Science and Engineering, University of California at Berkeley, Berkeley, California 94720

Received April 27, 2007; Revised Manuscript Received May 18, 2007

ABSTRACT

The infiltration (impregnation) of nanoscale particles, forming connected networks, into solid oxide fuel cell electrodes, has been shown to lead to considerable benefit in performance. Porous electrode skeletons (backbones), consisting of electrolyte material such as YSZ, when infiltrated, delivered results comparable to those of the standard Ni-YSZ and LSM-YSZ electrode configurations. Additionally, the performances of both single component mixed ionic electron conductor and of composite electrodes have been significantly enhanced by the connected nanoscale particle networks formed by infiltration.

Nanoscale materials (<100 nm) are receiving increased interest for application in devices where their unusual properties may possibly be exploited.[1,2] In solid oxide fuel cells (SOFCs) they can be added as catalyst, where it has been theorized that the advantageous catalytic properties of nanosized oxides relate to an enhanced surface vacancy concentration and increased ionic and electronic conductivities.[3−6] However, due to the elevated operating temperatures found in modern SOFCs, 500−750 °C, the use of entirely nanostructured components would undoubtedly lead to structural instability. Hence, nanoparticles have been incorporated in conjunction with more stable micrometer-sized supporting functional architectures.

The use of metal components in SOFC design has shifted system operating temperatures to 500−750 °C,[7] away from the ∼1000 °C systems initially adopted by Westinghouse and others.[8] The penalty is that SOFC performance decreases significantly at these lower operating temperatures. Particularly, it is the oxygen reduction reaction in the conventional SOFC cathode, a composite of LSM and YSZ, which is limiting at these intermediate temperatures.[9]

To enhance electrode performance at the lower operating temperatures, nanoparticulates are added to the internal surfaces of the porous electrodes to enhance some aspect of the electrode processes.[10−14] The nanoparticulates are typically added through processes that involve the precipitation of a metal salt in the pores of the electrodes, and their subsequent decomposition, to generate the desired nanoparticulate metallic or oxide catalyst. This method of electrode enhancement has proved reasonably successful. Additionally, it has been found that higher electrode loading of nanoparticulate catalysts further increases performance. In a review of such work by Jiang et al.[15] it is noted that repeating impregnation steps, leading to a connected network of nanoparticulates, provides substantially improved electrode performance. Unfortunately, the particle distribution produced by typical infiltration methods necessitates a large number of repetitions to produce a connected network of nanoparticulates, causing pore filling besides the intended coating of pore walls. Progressive filling of the pores has the drawback of causing gas diffusion limitations within the electrodes, which in turn limit performance at higher current densities. It would therefore be advantageous to engineer a uniform networked nanoparticulate layer within the electrodes, involving a minimal number of processing steps.

Previously, uniform and continuous networks of nanoparticulates were incorporated into porous electrodes by infiltration.[16−18] Importantly, the infiltration could be completed in a single processing step on both electrodes. Additionally, since the method is independent of all other processing steps, it can be preformed at lower temperatures, allowing for the use of otherwise reactive nanoparticulate catalysts.

The engineering of enhanced SOFC electrodes through the incorporation of networked nanoparticulate layers is more generally elaborated below. Advances in infiltration methods as well as their application to three SOFC electrode classes will be discussed. A single-step method is demonstrated, which not only improves performance in both fuel and air

† Materials Sciences Division, Lawrence Berkeley National Laboratory.
‡ Department of Materials Science and Engineering, University of California at Berkeley.

10.1021/nl071007i CCC: $37.00
Published on Web 06/09/2007

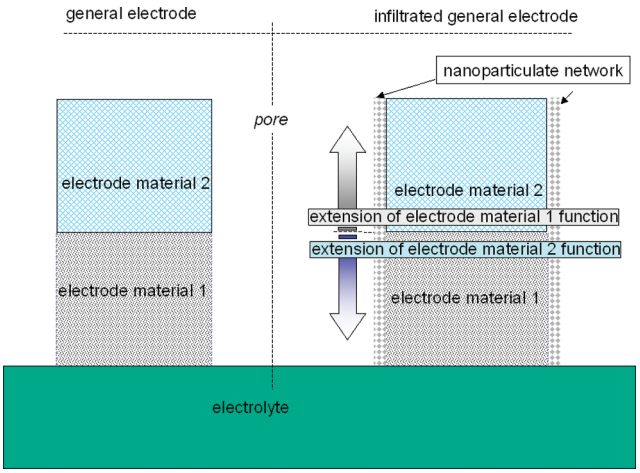

Figure 1. Cross-sectional illustration of nanoparticulate infiltration into a general composite electrode.

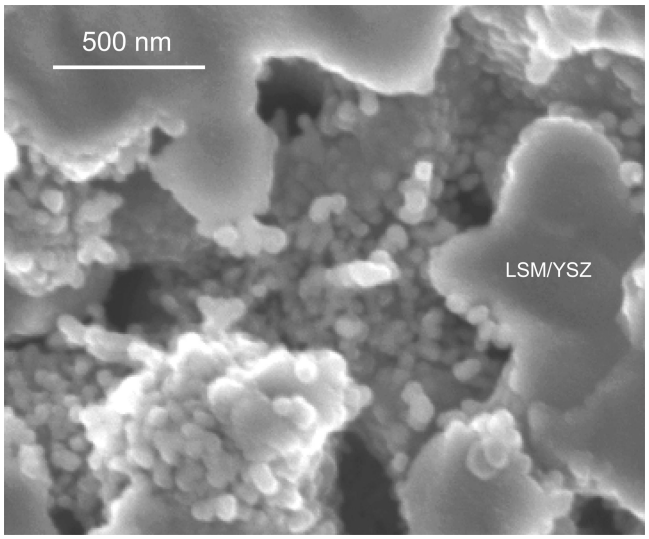

Figure 2. Secondary electron micrograph of conventional LSM-YSZ cermet air electrode infiltrated with YDC.

electrodes but additionally decreases the rate-limiting step in the cathode's oxygen reduction reaction at intermediate temperatures. The engineering of electrodes to such a level has broad implications for the improvement of SOFC performance.

Results and Discussion. In Figure 1 schematic illustrations of both a general and a nanostructured SOFC electrode are shown. The schematic can be used to describe the three classes of SOFC electrodes: (a) porous electrolyte backbones with infiltrated electrocatalyst; (b) single-component mixed ionic electronic conductor (MIEC) backbones; (c) composite electrodes backbones. Both the nanoscale component of the electrode and the micronscale backbone grains, which they are built on, serve a distinct purpose within each of the SOFC electrode classes. These functions are listed in Table 1 and will be further described in the following sections.

An important advance in the single-step infiltration procedure involved the modification of the chain length of the surfactant, Triton X, from $n \sim 10$ for Triton X-100 to $n \sim 5$ for Triton X-45. Assuming that micelles form in the precursor solutions and that the contents of the micelles are similar, a switch to shorter chain length would yield a considerable increase in material deposited by the infiltration. This decrease in surfactant chain length has facilitated the formation of well-connected nanoparticulate networks in a single step within less open electrodes. A conventional LSM-YSZ composite air electrode infiltrated with this improved method is shown in Figure 2, showing nearly complete coverage in a single step as compared to earlier efforts where the infiltrated electrodes were of highly porous electrodes.[17,18] With the ability to form well-connected nanoparticulate networks in a single processing step within conventional electrodes, focus can be shifted to decreasing the size of the nanonparticles, so as to exploit further the distinct properties that can be achieved at the nanoscale. For example, changes in infiltration procedure such as decreasing the concentration of the precursor solution, altering reaction rates, modifying the pH, or exploring other surfactants can yield micelles of the proper constitution to synthesize smaller nanoparticles within the porous electrodes.

(A) Infiltrated Porous Electrolyte Backbone Electrodes. Infiltration of porous electrodes is used to avoid solid-state reaction between the electrolyte and electrode materials that may otherwise occur at the elevated processing temperatures (~1100−1300 °C) needed to sinter such structures. One type of backbone for such electrodes, as can be visualized using Figure 1, would consist of the backbone grains being composed of the same material as the electrolyte. However, since electrolyte material usually serves no catalytic purpose and only provides an ion-conducting pathway, it is necessary to infiltrate a second material, which can form the electron pathways as well as the electrocatalytic sites within the electrode.

The main advantage in this case is the ability to infiltrate superior electrocatalysts. As is shown in Figure 3, an LSM-infiltrated electrocatalyst is compared to a superior LSF infiltrated electrocatalyst. LSM has been the material of choice in composite air electrodes because of its minimal interactions with YSZ at the elevated processing temperatures; however, it is a relatively poor electrocatalyst at

Table 1. Function of Backbone and Nanoparticles with in Each Electrode Class

porous electrode class	backbone function	nanoparticle functions
single component electrolyte composition	oxygen ion conduction	global electron supply, electrocatalyst
MIEC	oxygen ion and electron conduction, electrocatalyst	local oxygen ion conductivity, electrocatalyst
composite	global oxygen ion and electron conductivity, electrocatalyst	local oxygen ion and electron conductivity, electrocatalyst

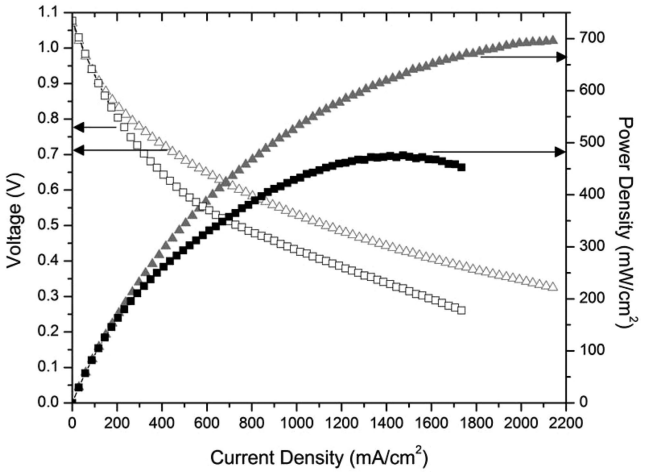

Figure 3. 700 °C performance of anode supported cell with porous YSZ air electrode infiltrated with LSM (■) or LSF (▲). The power density at 0.7 V is about 15% higher for LSF compared to LSM infiltrated backbones.

intermediate operating temperatures. Therefore, since the infiltration procedure only requires low-temperature sintering, 600−1000 °C, a reactive[19] but otherwise effective electrocatalyst[20] such as LSF can be used. In the $I-V$ cure in Figure 3, the enhanced electrocatalytic activity is illustrated by both the decreased overvoltage and the lower slope of the porous YSZ electrode activated by LSF infiltration.

(B) Infiltrated MIEC Backbone Electrodes. A major reason for LSF's superior electrocatalyic activity at lower operating temperatures is its mixed conductivity. The ability of MIECs to provide both electron and oxygen ion conduction pathways through an electrode, allows them to be utilized as single-component electrodes. To visualize these electrodes, consider both electrode grains to be composed of the MIEC in Figure 1. Even though MIEC electrodes are better electrocatalysts than LSM at intermediate temperatures, they can be improved by infiltration, as seen in Figure 4. Alternating current impedance characteristics of a LaSrCoFe (LSCF) symmetric cell provided by H. C. Stark are shown before and after the infiltration with nanoparticulate $Y_{0.2}Ce_{0.8}O_{1.9}$ (YDC). Since LSCF already provides sufficient electronic conductivity, it only stands to benefit from the ionic conductivity of the infiltrated YDC and possibly from additional catalysis.[21] The enhanced ionic conductivity in the electrode away from the electrolyte surface can be seen by the decrease in ohmic resistance in the Nyquist plot, Figure 4a, and by the decrease in the maximum phase shift of the high frequency arc of the Bode plot (∼10^2 Hz) Figure 4b. Additionally, there is a decrease in the phase angle (θ) of the low frequency arc of the bode plot (∼1 Hz), Figure 4b, indicating that even LSFC, a good electrocatalyst at intermediate operating temperatures, can be catalytically enhanced by infiltrated nanoparticles.

(C) Composite Backbone Electrodes. As for MIEC electrodes, the incorporation of nanoparticulate networks into working electrodes can produce added electrocatalysis, but more importantly in the case of composite electrodes, it can expand the strict triple phase boundary (TPB) reaction area

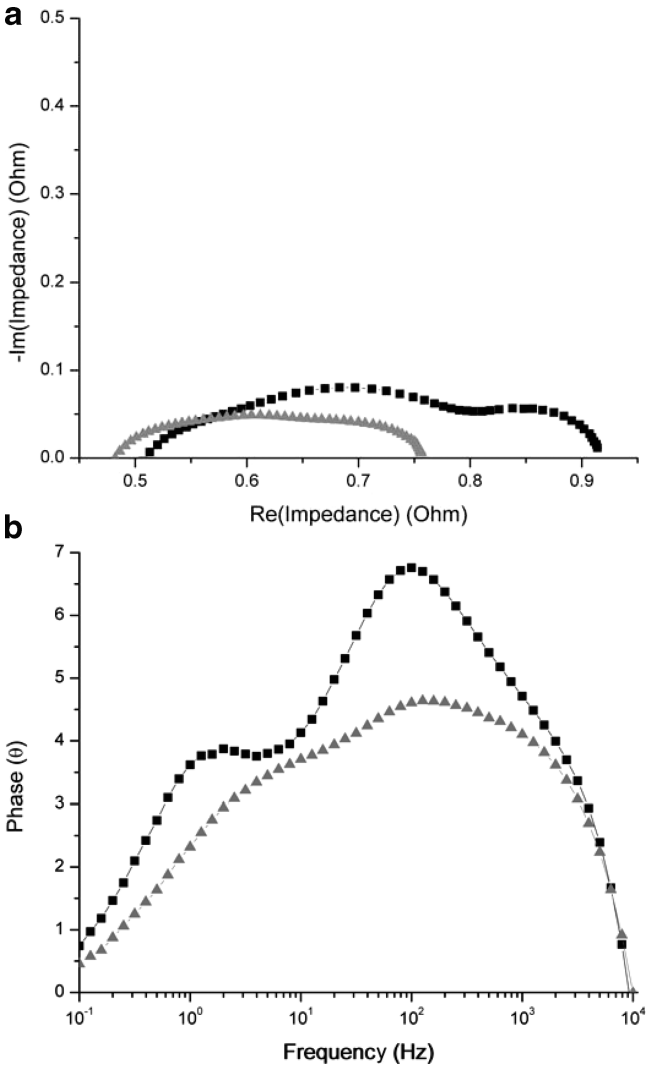

Figure 4. 700 °C ac impedance characteristics of electrolyte supported LSCF symmetric cell at OCV: (a) Nyquist and (b) Bode plots for cathode before (■) and after (▲) infiltrating with YDC.

typical for composite electrodes. Following Figure 1, the electrode is now composed of both electrode and electrolyte grains, providing percolative networks for both electronic and ionic conduction, respectively. The nanoparticulate chosen for infiltration was YDC. YDC has a high ionic conductivity[4] as well as sufficient electronic conductivity, especially in nanoparticulate form,[3,5,22] as has been demonstrated in the case of ceria, allowing for both ionic and electronic extension of the TPBs. Because composite electrodes already possess built-in electronic and ionic percolation networks through the electrode, the nanoparticulate YDC network layer does not need to be continuous throughout the electrode, since only short-range extension at the grain level dimension is needed. This significantly decreases the dependence of the cell on the morphological stability of the nanonparticulate networks, because a structurally stable backbone is already present.

Air Electrodes. Dramatic improvements in performance of a standard LSM-YSZ cathode are directly evident in the ac impedance characteristics, Figure 5. After infiltration with YDC, the Nyquist plot, Figure 5a, reduced in size to less

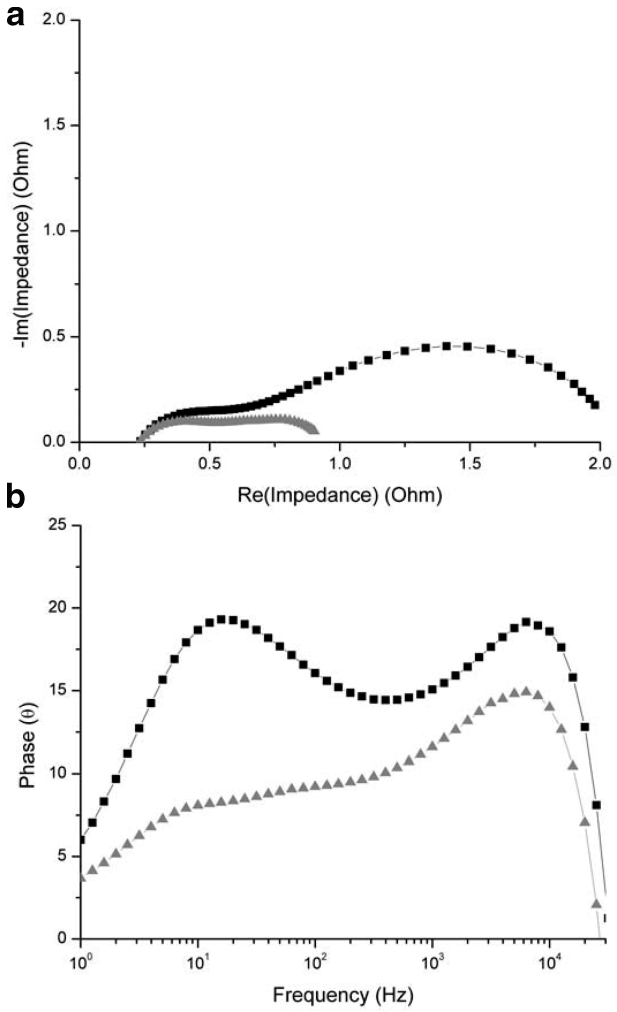

Figure 5. 700 °C ac impedance characteristics of anode-supported cell with LSM-YSZ cathode: (a) Nyquist and (b) Bode plots before (■) and after (▲) infiltration of YDC.

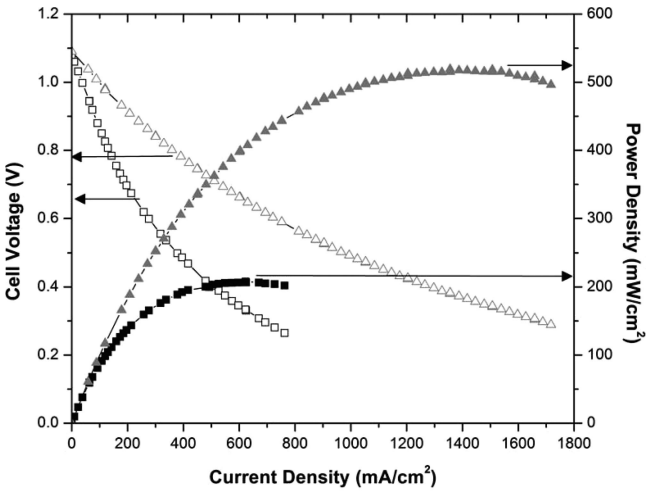

Figure 6. Enhancement of anode supported LSM-YSZ cathode before (■) and after (▲) infiltration of YDC, at 700 °C.

than 50% of its original form. The lowering in overall cell impedance is more readily seen in the Bode plot which explicitly shows frequency information, Figure 5b. There is an overall decrease in the phase angle (θ) after infiltration, for both the intermediate ~10 Hz and high ~10^4 Hz frequency peaks, with the intermediate frequency peak at ~10 Hz most drastically reduced. This intermediate frequency peak is usually associated with slow surface kinetics on the LSM-YSZ air electrode.[23,24] The strong decrease in the phase angle and in the overall impedance at this frequency following infiltration suggests that the enhanced microstructure minimizes the rate-limiting step in the reduction reaction within LSM-YSZ cathodes.

The result of the infiltration is a dramatic increase in cell performance, Figure 6. Even though the increase in peak power density from 208 to 519 mW/cm^2 before and after infiltration, respectively, is impressive, the most significant result of the infiltration is a dramatic increase in the power densities at low overpotentials. The cell shows a drastic enhancement of power density at 0.7 V from ~135 mW/cm^2 before infiltration to ~370 mW/cm^2 after infiltration. This decrease in "activation" losses is a marked improvement compared to infiltrated systems with isolated nanoparticulates.[12,13]

Fuel Electrode. Though the largest improvements in performance at intermediate operating temperatures stand to be made within air electrodes, significant improvement in fuel electrode ac impedance characteristics at OCV are evident following infiltration of $Sm_{0.2}Ce_{0.8}O_{1.9}$ (SDC), Figure 7. Unlike for the air electrodes, it is the high-frequency peak at ~10^4 Hz that correlates with the pronounced decrease in the overall cell impedance seen in the Nyquist plot, Figure 7a. A decrease in phase angle (θ) at high frequencies is common to both air, Figure 5b, and fuel electrodes, Figure 7b, suggesting a common origin. While a number of electrode-specific processes have been associated with this high-frequency peak, they can be broadly grouped into the category of charge-transfer processes within the electrodes.[24−26] As described earlier, the enhanced microstructure produced by the infiltration method will provide additional pathways through the electrodes, in essence minimizing the pathway for charge transfer, producing an increase in overall cell reaction area that can be well described by the model developed by. Lu et al.[12]

While the improvement was seen in the cell's ac impedance characteristics at OCV after infiltration, it does not translate into significant improvement in cell performance at low overvoltages, Figure 8. However, the infiltration produces a measurable increase in peak power density, from ~348 to ~403 mW/cm^2.

While the increase in fuel electrode performance is the most immediate benefit of the SDC infiltration, a more vital result is the significant increase in sulfur tolerance that is obtained. A number of cells have been tested and have shown sustained sulfur tolerance up to 40 ppm H_2S using the conventional Ni-YSZ material set infiltrated with doped and undoped ceria.[27] These preliminary tests indicate that it is possible to allow for the use of any commercial natural gas and promises that with further optimization of the anode microstructure and infiltration composition, stable sulfur tolerant anodes can be achieved using the conventional composite Ni-YSZ anodes. Additionally, the infiltration of

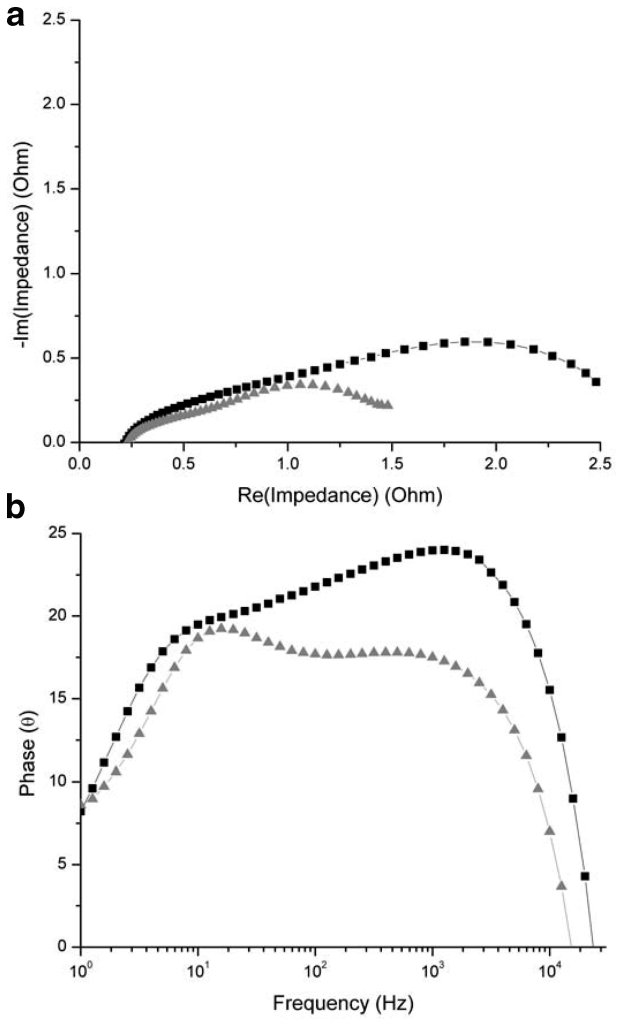

Figure 7. 700 °C ac impedance characteristics of anode-supported cell with a Ni-SSZ anode at OCV: (a) Nyquist and (b) Bode plots before (■) and after (▲) anode infiltration with SDC.

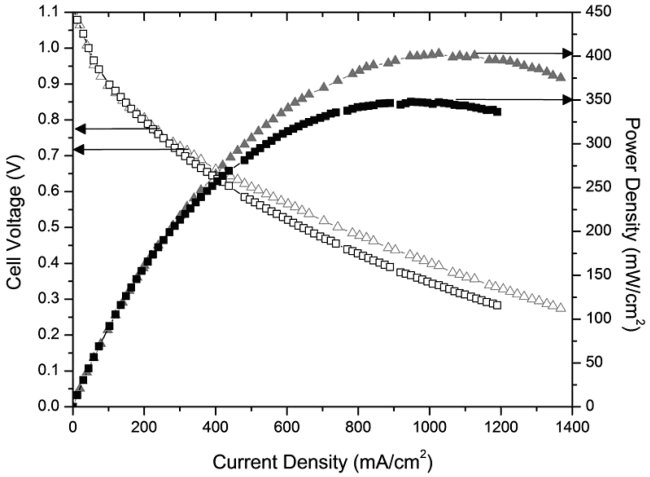

Figure 8. Enhancement of anode supported cell before (■) and after (▲) infiltration of anode with SDC, at 700 °C.

ceria can aid the stability of Ni-YSZ fuel electrodes by preventing sintering, grain growth and agglomeration of the Ni phase,[15] as well as providing the ability to directly reform hydrocarbons.[6,11] Therefore, because doped ceria infiltration can enhance both the air and the fuel electrodes performances, it should be the preferred choice for single-step infiltration of both SOFC electrodes, while at the same time decreasing manufacturing time and cost.

The stability of the nanostructured SOFC electrodes under the fuel cell operating conditions is of potential concern. However, extended stability has been demonstrated for several systems: LSM-infiltrated porous electrolyte backbones have shown over 500 h of continued performance enhancements at 650 °C;[18] ceria-infiltrated Ni-YSZ fuel electrodes, in humidified hydrogen containing significant concentrations of sulfur, were stable for over 500 h at 700 °C;[27] and doped ceria-infiltrated LSM-YSZ air electrodes have been stable at 700 °C in the 100+ hour tests conducted to date.

Conclusion. A single-step infiltration method, producing connected nanoparticulate networks in porous SOFC backbone electrodes, improves both air and fuel electrode performance.

The nanoscale nature of the infiltrated material has shown advantages in enhancing all three electrode classes and is expected to yield further benefits with progress in decreasing infiltrated nanoparticle size.

Acknowledgment. This work was supported by the U.S. Department of Energy's (DOE) Solid State Energy Conversion Alliance (SECA) and by the U.S. Department of Energy under Contract # DE-AC02-05CH11231. The authors thank H. C. Starck for supplying LSCF symmetric cells.

Supporting Information Available: Experimental details describing the three types of cell configurations that were prepared and examined This material is available free of charge via the Internet at http://pubs.acs.org.

References

(1) Sata, N.; Eberman, K.; Eberl, K.; Maier, J. *Nature* **2000**, *408* (6815), 946−949.
(2) Gu, Q.; Falk, A.; Wu, J.; Ouyang, L.; Park, H. *Nano Lett.* **2007**, *7* (2), 363−366.
(3) Tschope, A.; Birringer, R. *J. Electroceram.* **2001**, *7* (3), 169.
(4) Van Herle, J.; Horita, T.; Kawada, T.; Sakai, N.; Yokokawa, H.; Dokiya, M. *J. Eur. Ceram. Soc.* **1996**, *16* (9), 961−973.
(5) Tschope, A.; Kilassonia, S.; Zapp, B.; Birringer, R. *Solid State Ionics* **2002**, *149* (3−4), 261.
(6) Laosiripojana, N.; Assabumrungrat, S. *Chem. Eng. Sci.* **2006**, *61* (8), 2540−2549.
(7) Steele, B. C. H.; Heinzel, A. *Nature* **2001**, *414* (6861), 345−352.
(8) Feduska, W.; Isenberg, A. O. *J. Power Sources* **1983**, *10* (1), 89−102.
(9) Murray, E. P.; Tsai, T.; Barnett, S. A. *Nature* **1999**, *400* (6745), 649−651.
(10) Sahibzada, M.; Benson, S. J.; Rudkin, R. A.; Kilner, J. A. *Solid State Ionics* **1998**, 113−115, 285.
(11) Huang, B.; Ye, X. F.; Wang, S. R.; Nie, H. W.; Shi, J.; Hu, Q.; Qian, J. Q.; Sun, X. F.; Wen, T. L. *J. Power Sources* **2006**, *162*, (2 SPEC ISS), 1172−1181.
(12) Lu, C.; Sholklapper, T. Z.; Jacobson, C. P.; Visco, S. J.; De Jonghe, L. C. *J. Electrochem. Soc.* **2006**, *153* (6), 1115−1119.
(13) Yamahara, K.; Jacobson, C. P.; Visco, S. J.; Zhang, X.-F.; De Jonghe, L. C. *Solid State Ionics* **2005**, *176* (3−4), 275−279.
(14) Craciun, R.; Park, S.; Gorte, R. J.; Vohs, J. M.; Wang, C.; Worrell, W. L. *J. Electrochem. Soc.* **1999**, *146* (11), 4019.
(15) Jiang, S. P. *Mater. Sci. Eng., A* **2006**, *418* (1), 199−210.

(16) Kurokawa, H.; Yang, L.; Jacobson, C. P.; De Jonghe, L. C.; Visco, S. J. *J. Power Sources* **2007**, *164* (2), 510−518.
(17) Sholklapper, T. Z.; Lu, C.; Jacobson, C. P.; Visco, S. J.; De Jonghe, L. C. *Electrochem. Solid-State Lett.* **2006**, *9* (8), 376−378.
(18) Sholklapper, T. Z.; Radmilovic, V.; Jacobson, C. P.; Visco, S. J.; De Jonghe, L. C. *Electrochem. Solid-State Lett.* **2007**, *10* (4), B74−B76.
(19) Anderson, M. D.; Stevenson, J. W.; Simner, S. P. *J. Power Sources* **2004**, *129* (2), 188−192.
(20) Simner, S. P.; Bonnett, J. F.; Canfield, N. L.; Meinhardt, K. D.; Shelton, J. P.; Sprenkle, V. L.; Stevenson, J. W. *J. Power Sources* **2003**, *113* (1), 1−10.
(21) Wang, H. B.; Song, H. Z.; Xia, C. R.; Peng, D. K.; Meng, G. Y. *Mater. Res. Bull.* **2000**, *35* (14−15), 2363−2370.
(22) Xiong, Y.; Yamaji, K.; Horita, T.; Sakai, N.; Yokokawa, H. *J. Electrochem. Soc.* **2002**, *149* (11), 450−454.
(23) Chen, X. J.; Khor, K. A.; Chan, S. H. *J. Power Sources* **2003**, *123* (1), 17−25.
(24) Kim, J. D.; Kim, G. D.; Moon, J. W.; Park, Y. I.; Lee, W. H.; Kobayashi, K.; Nagai, M.; Kim, C. E. *Solid State Ionics* **2001**, *143* (3−4), 379.
(25) Primdahl, S.; Mogensen, M. *J. Electrochem. Soc.* **1997**, *144* (10), 3409.
(26) Primdahl, S.; Mogensen, M. *J. Electrochem. Soc.* **1999**, *146* (8), 2827.
(27) Kurokawa, H.; Sholklapper, T. Z.; Jacobson, C. P.; Visco, S. J.; De Jonghe, L. C. *Electrochem. Solid State Lett.*, in press.

NL071007I